Reductions in Strong Upwelling-Favorable Wind Events in the Pliocene

Zhiyuan Li[1], Yangcheng Luo[2], Nathan Arnold[3], Eli Tziperman[4]

[1]Dept. of Atmospheric and Oceanic Sciences, School of Physics, Peking University, Beijing, China
[2]Division of Geological and Planetary Sciences, Caltech, Pasadena, CA, USA
[3]Global Modeling and Assimilation Office, NASA Goddard Space Flight Center, Greenbelt, Maryland, USA
[4]Department of Earth and Planetary Sciences and Planetary Sciences and School of Engineering, Harvard University, Cambridge, Massachusetts, USA

Key Points:

- Proxy records of the Pliocene show significant warming of SST at mid-latitude upwelling sites.
- Strong transient upwelling-favorable wind events that drive much of the SST cooling at present are reduced given Pliocene SST estimates.
- This reduction is closely related to changes in anticyclonic atmospheric activity in a warmer climate.

Corresponding author: Eli Tziperman, Department of Earth and Planetary Sciences and School of Engineering and Applied Sciences, Harvard University, 20 Oxford St, Cambridge, MA 02138-2902, USA. eli@eps.harvard.edu

Corresponding author: Nathan Arnold, Global Modeling and Assimilation Office, NASA Goddard Space Flight Center, Mail Code: 610.1, Greenbelt, Maryland, 20771, USA, nathan.arnold@nasa.gov

This article has been accepted for publication and undergone full peer review but has not been through the copyediting, typesetting, pagination and proofreading process which may lead to differences between this version and the Version of Record. Please cite this article as doi: 10.1029/2019PA003760

Abstract

Proxy records of the Pliocene show significant warm anomalies of sea surface temperatures (SST) near mid-latitude upwelling sites at the eastern boundaries of the Pacific and Atlantic Oceans. Weaker upwelling-favorable mean winds or a deeper thermocline have been proposed as explanations, yet the mechanisms involved are still not clear and the dramatic warmings of up to 9°C are only partially accounted for. Here we quantify the response of strong *transient* upwelling-favorable wind events, defined to have a wind velocity over 5 m s^{-1} and a duration of at least three days, to two reconstructions of Pliocene SST. Such events are responsible for much of the modern upwelling SST signal and may therefore be a more relevant measure than the climatological winds. We find that both the amplitude and duration of upwelling-favorable events are reduced in the Pliocene scenarios. Using PRISM4 SST, we find an annual reduction in upwelling flux between 7.4%-13.2%, depending on model resolution. With an idealized Pliocene SST, the reduction in upwelling flux is between 46.7%-50.3%. This reduction is shown to be closely related to changes in anticyclonic atmospheric activity, associated in turn with a weaker large-scale meridional SST gradient.

1 Introduction

The early-to-mid Pliocene, 5.3-3.1 million years ago, was the most recent period of sustained global warmth and is considered an analogue for a future global warming scenario (Chandler, Rind, & Thompson, 1994; H. Dowsett, Barron, & Poore, 1996; H. Dowsett & Robinson, 2009; H. J. Dowsett et al., 2012). Proxy records and modeling results indicate that global average surface temperature was about 3-4°C warmer than at present (H. J. Dowsett et al., 2013, 2011; O'Brien et al., 2014). The early Pliocene is believed to have been characterized by substantially lower meridional and zonal temperature gradients, and the sea surface temperature (SST) of the west Pacific warm pool was similar to present (A. Fedorov et al., 2013; A. Haywood et al., 2012). The average SST difference between the east and the west sides of the equatorial Pacific Ocean was only 1.5± 0.9°C and there was a deep thermocline in the eastern Pacific Ocean. Due to their similarity to a modern El Niño event, these conditions have been termed a "permanent El Niño" (N. Burls & Fedorov, 2014; Dekens, Ravelo, McCarthy, & Edwards, 2008; A. V. Fedorov, Brierley, & Emanuel, 2010; A. M. Haywood, Valdes, & Peck, 2007; Ravelo, Dekens, & McCarthy, 2006). We note that some recent SST proxy reconstructions suggest that the zonal SST gradient during the early Pliocene was, in fact, comparable to or only moderately smaller than modern values (Tierney, Haywood, Feng, Bhattacharya, & Otto-Bliesner, 2019; Zhang, Pagani, & Liu, 2014).

Another interesting feature during the Pliocene, relevant to this work, is the anomalously high SST in mid-latitude upwelling regions. Multiple proxies have found that SSTs at mid-latitude upwelling sites such as the California, Humboldt, Canary and Benguela, were significantly warmer than present, by 3-9°C, indicating a major shift in these cold upwelling zones during 4.6-3 Ma (Brierley et al., 2009; Dekens, Ravelo, & McCarthy, 2007; Herbert & Schuffert, 1998; LaRiviere et al., 2012; Marlow, Lange, Wefer, & Rosell-Mele, 2000). Upwelling regions play a significant role in maintaining ocean biodiversity, encompass a large fraction of fisheries, and regulate regional and basin scale climate (Lau & Shen, 1988; Pauly & Christensen, 1995; Seager et al., 2003). How these upwelling systems will respond to a warmer climate is therefore of great interest.

Previous studies suggested several mechanisms for the disappearance of the cold upwelling zones during the Pliocene. One is that the thermocline was deeper, such that the upwelling brought up relatively warmer, above thermocline, water to the ocean surface compared with the modern case (Chaisson & Ravelo, 2000; Ford, Ravelo, Dekens, LaRiviere, & Wara, 2015; Wara, Ravelo, & Delaney, 2005). It has been proposed that a tectonic process such as the closing of the Panama Seaway influencing the intermedi-

ate water (Haug, Sigman, Tiedemann, Pedersen, & Sarnthein, 1999; Steph et al., 2010), or a northward movement of New Guinea and the restriction of the Indonesian Seaway (Cane & Molnar, 2001), could have led to the shallower modern thermocline (A. Fedorov et al., 2006), although these explanations still leave significant gaps in terms of the detailed mechanisms involved. It has also been proposed that the reduced meridional SST gradient would result in a more locally balanced energy budget, thus causing a deeper ventilated thermocline during the early-to-mid Pliocene (Boccaletti, Pacanowski, Philander, & Fedorov, 2004; Philander & Fedorov, 2003).

Another possibility is that a smaller equator-to-pole temperature gradient and a weaker Hadley Circulation could reduce the intensity, or shift the location, of upwelling-favorable wind at mid-latitude areas (Arnold & Tziperman, 2015; Lu, Vecchi, & Reichler, 2007; Tziperman & Farrell, 2009). Arnold and Tziperman (2015) used an atmospheric general circulation model (AGCM) to simulate the surface wind stress in both modern and Pliocene scenarios with a horizontal grid spacing of roughly 1° and a prescribed SST. They calculated the mean climatological alongshore wind stress (AWS) and wind stress curl to estimate the coastal and mid-ocean upwelling mass fluxes. They found reductions of 10% to 50% in both coastal upwelling driven by AWS and offshore upwelling driven by wind stress curl. However, such reductions alone appear to be insufficient to explain the anomalies suggested by temperature proxies (Miller & Tziperman, 2017).

Although upwelling is a coupled atmosphere-ocean process, the use of prescribed SST is justified by the difference in spatial scale between the wind field driving the upwelling, and the SST anomalies that result. While the SST signal of upwelling extends at most a few hundred kilometers from the coast, the along-shore wind stress is typically part of a basin-scale anticyclonic circulation spanning several thousand km. Such circulations depend more on the large-scale SST gradients than the local SST associated with upwelling. It is thus possible to consider how the large-scale differences in Pliocene SST would impact the coastal winds, while neglecting the relatively small feedback from the local SST. This approach, of asking how the large-scale SST affects the wind, complements studies that use a dynamical ocean model with prescribed winds to study the local ocean upwelling response (Miller & Tziperman, 2017). Eventually, of course, the problem would need to be tackled by a fully coupled ocean-atmosphere model. We note that current coupled climate models typically use ocean grid spacing that is too coarse to resolve coastal upwelling processes, and consequently find it difficult to reproduce the warmer upwelling regions in Pliocene simulations (H. J. Dowsett et al., 2013; A. Fedorov et al., 2013; A. Haywood et al., 2012).

At present-day, the narrow strip of cold upwelling water is confined within 10-50 km of the coast (Allen, 1980; Enriquez & Friehe, 1995; Hurlburt & Thompson, 1973; Renault et al., 2012; Small, Curchitser, Hedstrom, Kauffman, & Large, 2015). The occurrence of nearshore drop-off of the wind speed leads to an enhanced wind stress curl there, which favors upward Ekman pumping (Capet, Marchesiello, & McWilliams, 2004; Enriquez & Friehe, 1995). According to Winant and Dorman (1997), an increase in atmospheric model resolution from 1° to 0.2° improves the simulation of this drop off and therefore increases the simulated wind stress curl off California by a factor of three. This motivates our use in this paper of several model resolutions, including one at 0.25°. The increased resolution does not change our results significantly, indicating numerical convergence and increasing the confidence in the results. Furthermore, previous studies considered only the climatological monthly mean alongshore wind stress and wind stress curl to estimate the upwelling mass flux. However, according to some studies of the biological productivity and SSTs at the California upwelling zone, while the Ekman response occurs in less than a day, a wind forcing with a duration of at least three days and an amplitude of 5 $\mathrm{m\,s^{-1}}$ is required for the cold, nutrient-rich water to reach the surface (Botsford, Lawrence, Dever, Hastings, & Largier, 2006; Dugdale, Wilkerson, Hogue, & Marchi, 2006; García-Reyes & Largier, 2010). One may therefore conclude that the proxy data,

relying on biological activity to record SST, is mostly affected by strong upwelling-favorable wind events, and this indeed is our focus here.

We build on the work of Arnold and Tziperman (2015), using higher resolution simulations and considering the role of wind variability and strong wind events, focusing on the California upwelling site. We find a large reduction in the number of strong upwelling wind events in simulations with Pliocene SST. We further show that strong upwelling events are always accompanied by anticyclones over the northeast Pacific Ocean, and that both the frequency and amplitude of those upwelling-favorable anticyclones is reduced in the Pliocene scenarios.

2 Methods

2.1 Pliocene Simulations

Here we analyze three SST configurations meant to represent the modern era (Modern), the mid-Pliocene (PRISM4) and an idealized early Pliocene case (Idealized). The modern SST is based on the climatology from the Hadley Centre Sea Ice and Sea Surface Temperature (HadISST) data set (Rayner et al., 2003). The mid-Pliocene case uses lower boundary conditions from the Pliocene Reconstruction Interpretation and Synoptic Mapping (PRISM4) data set representing the mid-Piacenzian (3.29-2.97Ma) (H. Dowsett & Robinson, 2009). It is a palaeoenvironmental reconstruction containing data for palaeogeography, land, vegetation, soils, lakes, SST and sea-ice. The Idealized case SST represents an extreme idealization of the warm, low-gradient conditions prevailing in the early Pliocene (4.2-4 Ma) from Brierley et al. (2009). The three SST distributions are shown in the supporting information Fig. S1.

We use the NCAR Community Atmosphere Model (CAM) version 5, a state-of-the-art GCM used for future climate projections, and used previously to study the Pliocene (Arnold & Tziperman, 2015; Koll & Abbot, 2013). Specifically, we use the land model CLM4.0 (Lawrence et al., 2011; Oleson et al., 2010) and atmospheric model CAM-5.3 (Neale et al., 2010, 2012) from CESM-1_2_2_1. The land vegetation and topography are set to their modern values, as we focus on the effects of the SST, future studies would need to examine the effects of the land conditions as well. The bulk aerosols model is used, Milankovitch forcing is set to modern values and CO_2 is set, as in Arnold and Tziperman (2015), to 355 ppm for modern and 405 ppm for the Pliocene simulations. For each scenario we run the model at several horizontal resolutions: (1) $0.23^\circ \times 0.31^\circ$ (component set f02_f02, hereafter referred to as the 0.25° resolution), allowing resolution of the coastal wind drop off near upwelling sites; (2) half a degree resolution ($0.47^\circ \times 0.63^\circ$, f05_f05) ; (3) 1 degree resolution ($0.9^\circ \times 1.25^\circ$, f09_f09). There are 30 levels in the vertical. We run the 0.25° model in all three scenarios for two years, the 0.5° for 10 years, and the 1° model for 20 years. The first year in each case is discarded to allow for spinup. Additional information on component sets is available at http://www.cesm.ucar.edu/models/cesm1.2/cesm/doc/modelnl/compsets.html.

2.2 Definition of the upwelling index

Upwelling can be divided into coastal and offshore fluxes. Coastal upwelling is caused by the alongshore wind stress (AWS) parallel to the shore which leads to off-coast horizontal transport and to a subsequent cold upwelling from below. Offshore upwelling, on the other hand, is caused by the divergence of surface water driven by wind stress curl. Thus, the expressions of coastal upwelling and offshore upwelling (Bakun & Nelson, 1991;

Marshall & Plumb, 2016) can be written as,

$$M_{coast} = \frac{\tau_{as}}{f}$$

$$M_{curl} = \frac{1}{f} \bigtriangledown \times \vec{\tau}.$$

Here $\vec{\tau}$ is the wind stress vector, τ_{as} is the "along-shore" component parallel to the coast and f refers to the Coriolis parameter. We follow the definition of offshore upwelling index used in Arnold and Tziperman (2015) by identifying the nearest coastal point to the Ocean Drilling Project sediment core site 1014 in the California Current System, and averaging offshore upwelling of all grid points within a box extending 150 km in each along-shore direction and 300 km from the coast out to sea. The Pliocene SST at this site was estimated to be 8.8°C warmer than modern (Dekens et al., 2007). The averaged index is then multiplied by 300 km to bring it to the same units as the coastal index, representing the integrated upwelling. The coastal upwelling index is defined based on the maximum along-shore wind within the box, which quantifies the magnitude of coastal upwelling.

2.3 Definition of strong upwelling events

Previous studies of Pliocene upwelling have used annual or monthly mean wind stress to calculate the intensity of upwelling. While equatorward alongshore wind of any magnitude forces coastal upwelling, there is a threshold at which a response in SST can be observed. Some studies defined a minimum duration (Botsford et al., 2006; Dugdale et al., 2006) of wind events required to bring cold deep water up to the surface, while others (Largier et al., 2006; Wilkerson, Lassiter, Dugdale, Marchi, & Hogue, 2006) consider a wind speed threshold of 5 m s^{-1}. Here, we define "strong" upwelling events to be those whose alongshore wind velocity exceeds 5 m s^{-1} and last at least three days. This is consistent with the findings of previous studies (Botsford et al., 2006; Dugdale et al., 2006; García-Reyes & Largier, 2010) that while the Ekman response occurs in less than a day, a wind forcing with a duration of at least three days is required for the cold, nutrient-rich water to reach the surface. We examine the sensitivity to the amplitude threshold of 5 m s^{-1} below.

2.4 Track analysis

To characterize anticyclone position and intensity, we use the TRACK program (Hodges, 1994), which can objectively identify features in a time sequence of meteorological data. Features are tracked through time to produce trajectories of the feature centers (Hodges, 1995). We use this approach to track the position and intensity of anticyclones using 6-hourly sea level pressure data and to better understand the reduction in strong upwelling events during the early-to-mid Pliocene. The intensity is defined relative to the large scale background at each time step which is removed by the spectral filter: the pressure is first decomposed into spherical harmonics and the coefficients for total wave numbers less than six are set to zero (Hodges, 1996) to remove the large-scale background.

2.5 Effects of model resolution

Simulations with the Community Atmosphere Model demonstrate that both the coastal upwelling index and offshore upwelling index increase with a finer resolution of approximately 0.25°. Supporting information Fig. S2 shows the topography around the upwelling site near California with 1°, 0.5° and 0.25° resolutions. The higher resolution and more realistic topography in the 0.25° simulation leads to a more realistic wind reduction there and therefore to a stronger wind stress curl near the coast, and therefore to a larger offshore upwelling index. The scatter plot of alongshore wind stress on distance from shore in Fig. S3 shows a stronger alongshore wind stress for the higher res-

olutions, that is also closer to the coast, which leads to a greater coastal upwelling index. Although the upwelling regions are better characterized by the 0.25° simulation, the reduction of upwelling index associated with Pliocene SST does not change significantly. For much of the following, we use the 1° simulations, as the longer simulation allows for more robust statistics. When possible, we show the results with the 0.25° and 0.5° simulations as well, which are seen to be consistent with the 1° model results, although their uncertainty is larger due to the shorter records.

3 Results

We divide the results into three parts. First, we repeat the experiments from Arnold and Tziperman (2015) at a higher model resolution which better resolves the wind decline toward the coast, to calculate the annual-averaged and monthly climatology of upwelling intensity for the different prescribed SST distributions. Second, we analyze the dependence of strong upwelling events on the SST. Third, we introduce TRACK analysis to further understand the reduction in strong upwelling wind events during the Pliocene and its relationship with anticyclonic weather systems.

3.1 High model resolution

The color shading panels on the top row of Fig. 1 show the annual mean upwelling mass flux per unit area, while the vectors show the surface wind stress, based on the 0.25° resolution model. The dots and boxes indicate the sediment core site and the 300 by 300 km area around it. These results are presented for the modern SST as well as for the differences between the two Pliocene scenarios and the modern scenario. The high resolution allows a better simulation of the structure of wind stress changes toward the coast, and the resulting strip of positive upwelling in the modern case is comparable to that seen in the QuikSCAT satellite observations. The difference plots show modest reductions in AWS and curl-driven upwelling with PRISM4 SST, and greater reductions with idealized SST. This result is consistent with the idealized scenario being an extreme version of the low-gradient Pliocene SST. The evaluation of statistical significance of the difference maps is based on Student's t test, and values that are not significant to within 95% are shown in white.

When the model resolution is increased from 1° to 0.25°, the reduction of annual mean coastal upwelling index relative to the modern scenario remains unchanged at 11.5% with PRISM4 SST, and increases slightly from 38.4% to 43.5% with idealized SST, as shown in Table 1. The reduction of the annual mean offshore upwelling index also increases from 7.3% to 11.0% and from 43.1% to 46.1% in the PRISM4 and idealized scenarios respectively. The 0.5° resolution model shows a similar sensitivity, also shown in Table 1, although with a smaller reduction of the off-shore index. Overall, the fractional changes in upwelling with Pliocene SST are similar to the lower resolutions of Arnold and Tziperman (2015). These results indicate that the modest fractional change in upwelling with Pliocene versus Modern SST is not an artifact of using a coarse resolution. Similar reductions can also be seen in the monthly indices for coastal upwelling and for offshore upwelling, shown in the bottom panels of Fig. 1. These results imply that a reduction in annual mean upwelling-favorable wind stress is unlikely to explain the Pliocene warm SST anomalies. Note that the wind reduction in the idealized SST case is much more dramatic than for the PRISM SST, consistent with the idealized SST being a fairly drastic sensitivity experiment, as well as with the stronger shift in cyclone location that account for upwelling wind events, as discussed below.

3.2 Strong upwelling events

However, the upwelling of cold, nutrient-rich water that supports biological productivity and colder SSTs at the California site requires upwelling-favorable wind forcing with a duration of at least three days and an amplitude larger than about 5 $\mathrm{m\,s^{-1}}$ (Botsford et al., 2006; Dugdale et al., 2006; García-Reyes & Largier, 2010). Therefore, rather than focusing on annual or monthly mean upwelling indices, we now consider such strong upwelling events using a time series of daily upwelling index. An example segment from the final year of the 1° simulation is shown in Fig. 2. The three lines show the daily value of the coastal upwelling index in the upper panel, and the offshore upwelling index in the lower panel, for the three SST scenarios. The upwelling caused by modern SST (blue line) forcing seems larger than the Pliocene SSTs (red and green line) and to persist for a longer period of time at higher values, although this is not obvious from the time series and is further quantified next. We note that Fig. S4 shows a comparable time series for the 0.25° model resolution, with similar results.

Fig. 3a shows the probability distribution functions of the upwelling indices for the three scenarios in the last 10 years of the 1.0° simulations. The number of days with large upwelling index values is reduced under the two Pliocene SST scenarios. The green curve representing the idealized Pliocene case is significantly lower than the blue one representing modern SST for higher values of the two indices. The same difference is also seen for the PRISM case and while the curve is consistently below that of the modern case for higher index value, the difference is not as large as in the idealized case, especially for the off-coastal index. Panels b and c show the distributions for the 0.5 and 0.25° resolutions. The distributions are qualitatively similar across resolutions, particularly for the offshore upwelling index. The model distributions of the coastal index are more similar to QuikSCAT as resolution increases, emphasizing the importance of a fine model grid in capturing coastal wind intensities.

We find that the total duration of events every year, the average duration of an event and the average intensity of an event, all decrease for Pliocene SSTs, while the frequency of events does not change dramatically, as shown in Table 2. The results in the Table are based on a definition of strong upwelling events as having an alongshore wind velocity exceeding 5 $\mathrm{m\ s^{-1}}$ and a duration of at least three days. We quantify the annual upwelling by adding up the coastal upwelling index for all days with strong upwelling events. Note that, using this definition, a majority of all days in the Modern and PRISM4 cases are flagged as strong events. We are reassured that the definition is reasonable in part due to the seasonality of implied upwelling (Fig. S5), which is consistent with observations (García-Reyes & Largier, 2010).

The total reduction in annual upwelling flux in Table 2 is found by multiplying the total number of strong upwelling days by the average upwelling flux during these days. This measure decreases with PRISM4 SST relative to modern by 13.2%, and with the idealized Pliocene SST by 47.0%. We also perform the same calculation for the 0.5° and 0.25° simulations: the reduction in coastal upwelling is 46.7% and 50.3%, respectively, with idealized SST, but only 10.5% and 7.4% with the PRISM4 SST. The qualitative similarity of these reductions across the three resolutions suggests the short simulation time of the 0.25° case does not render its statistics unreliable.

While the thresholds used here to define upwelling events are based on modern observational constraints as mentioned above, the Pliocene climate may have been very different and what constituted a significant upwelling event may have been different. Fig. S6 in the supplementary materials shows the results for different duration thresholds, using 2, 3 and 4 days, for the 1°, 0.5° and 0.25° resolution models. The number of events, total duration, average duration and average intensity show some dependence on the duration threshold, with the number of events showing the strongest dependence (decreasing with duration), yet the qualitative conclusions hold. Fig. S7 in the supplementary

materials shows the sensitivity to different amplitude thresholds, using the standard 5 m s^{-1} threshold and then changing it by ±20% and ±40%. The sensitivity of the number of events is not linear, because as the amplitude threshold is decreased, there are instances when two separate events are merged into one. Other than that the event statistics change with the threshold, but the overall picture is similar to that discussed above.

3.3 Understanding the reduction in strong events

To better understand the cause of the reduction in strong upwelling events, we consider the time evolution of selected events. The following analysis uses only the 1° simulations, but from the resolution independence noted above we expect the 0.25° and 0.5° results to be similar. Consider the sea level pressure and wind stress and offshore upwelling in the two largest coastal upwelling wind events from the modern run shown in Fig. 4. Although there are some differences in the pattern, we can see a strong anticyclonic high to the west of the upwelling site in both events, enhancing the along-shore wind velocity at the upwelling site. This leads us to hypothesize that changes to the behavior of such Northeast Pacific anticyclones may cause the reduction in upwelling at the California site during the Pliocene.

We therefore proceed to analyze the movement and location of subtropical anticyclones for the three different SSTs. Figure 5 shows the composite of sea level pressure and surface wind stress and offshore upwelling for all strong upwelling events in each scenario. Events in each case are defined using the same 5 m s^{-1}, 3-day criteria. The composite, being an average over many events, looks like an enhancement of the central pressure of the climatological anticyclonic subtropical high, and this enhancement is weaker in the Pliocene scenarios. There is also a low pressure center over the continental United States near California, whose magnitude does not change much for the different SST scenarios. The land-sea pressure gradient in mid-latitudes gets weaker for the higher SSTs, leading to a smaller alongshore upwelling-favorable wind stress and weaker offshore upwelling, resulting in an expected weakening of Pliocene upwelling events.

We next track the location and intensity of every anticyclone of our twenty year runs, based on 6-hourly output, in all three SST scenarios, using the TRACK Program (section 2.4). Fig. 6 presents the track point density in the modern scenario and the difference from the two Pliocene SST scenarios. The track point density quantifies the frequency of anticyclones, and is presented in units of $km^{-2}\ year^{-1}$, to make it independent of the model resolution. The subtropical high and polar high in both hemispheres are clearly characterized as areas of high track density in the upper panel, while most of the lower latitudes, where there are but few track points, appears white. The middle and bottom panels indicate that the density of anticyclones around 30° latitude decreases with PRISM4 SST while the density increases in higher and lower latitudes, and this change is even more obvious in the idealized SST case. These changes correspond to an expansion of the modern high track density subtropical areas both north and south in the warmer climates, as well as reduction of density over the subtropical high itself. Overall, these changes correspond to a reduction in the frequency of anticyclones that affect the upwelling around California Site 1014, consistent with the upwelling changes seen in the above analysis.

The TRACK analysis is also used to calculate the intensity of the anticyclones presented in Fig. 7, calculated as a sea level pressure anomaly relative to the background. The background is calculated by decomposing sea level pressure into spherical harmonics and setting the coefficients for total wave numbers larger than five to be zero. The difference maps between the Pliocene SSTs and the modern case show weaker anticyclones in the east Pacific Ocean and stronger ones in the west. A physical interpretation of these results is complicated, as differences in the average anticyclone intensity could reflect either an overall change in anticyclone energy, or a shift in the distribution of an-

ticyclone intensities. For example, a selective reduction in the number of weaker anticyclones would appear as an increase in average intensity, despite an overall reduction in the energy associated with anticyclones.

We conclude that the TRACK analysis demonstrates that both the frequency of occurrence and intensity of anticyclones that lead to upwelling-favorable winds near California decrease significantly with the increase of SST in the Pliocene, leading to the large reductions in strong upwelling events at the California site.

One factor that may contribute to the poleward shift of anticyclone activity is a weakening of the Hadley cell. The mean Hadley cell during the upwelling season (Feb-September) weakens in the Pliocene simulations without apparent latitudinal shifts (Fig. S8) and the precipitation weakens in the tropics and strengthens at mid-latitudes (Fig. S9). These results are consistent with the simulations of N. J. Burls and Fedorov (2017) who noted the limitations of using the Pliocene as an analogue of a future warming scenario. The shift of the anticyclone density is consistent with a weakening and poleward shift of the Hadley circulation seen in numerous climate change simulations. This Hadley expansion has been explained by tropical heating processes (Mitas & Clement, 2006), changes to atmosphere stability (Schneider, 1977), subtropical eddy dynamics (Walker & Schneider, 2006) and atmosphere moisture effects (Frierson, Held, & Zurita-Gotor, 2006; Lu et al., 2007).

A second factor potentially contributing to the anticyclone shift is a poleward shift in baroclinicity associated with the prescribed Pliocene SST. The meridional temperature gradient serves as the primary source of energy for anticyclonic storms, and it follows that reductions or shifts in that gradient may alter the position or intensity of the storm track. Figure S10 shows the absolute value of the meridional gradient in prescribed SST averaged zonally across the Pacific from 150°E to 120°W. The gradient is visibly reduced in midlatitudes in both Pliocene cases, with increases poleward of 45°N. This is consistent with the weakening and poleward shift found in the track analysis.

4 Conclusions

We examined the hypothesis that the warming of coastal mid latitude upwelling sites during the Pliocene was a result of change to the magnitude and frequency of strong upwelling-favorable wind events, rather than, or in addition to, changes to the mean winds or other ocean factors. We focus our analysis on the California upwelling zone with the expectation that the results may be applicable to other such mid-latitude upwelling sites. While the effects of coastal upwelling are felt over 100 km away from the coast (Spall & Schneider, 2016), the coastal upwelling zones themselves are very narrow, on the order of a 10-20 km, and it is important to correctly simulate the winds over such a narrow region. We therefore used a high atmospheric model resolution of 0.25° that allows to correctly simulate the decrease of the along-coast wind amplitude toward the coastline. We used two indices reflecting the magnitude of both coastal upwelling due to the wind amplitude, and offshore upwelling due to the wind curl, and examined extreme events in these indices for modern SST and for two Pliocene SST scenarios.

Our main result is that strong upwelling-favorable wind events are reduced more than the mean in Pliocene SST scenarios compared with the modern case. For example, depending on model resolution, the Idealized Pliocene SST resulted in a reduction of 46.7-50.3% in the annual coastal upwelling associated with strong events, but only a 37.3-43.5% reduction in the mean. We also showed that strong upwelling wind events are associated with anticyclonic atmospheric motions to the west of the upwelling site, and in order to understand the changes to the coastal upwelling wind events, we examined the effects of the Pliocene SST on mid-latitude anticyclone frequency and intensity. We track the position and intensity of anticyclones using 6-hourly sea level pressure (Hodges,

1995) and find a decrease of both intensity and duration of anticyclones that lead to upwelling-favorable winds events. Specifically, we show a weakening of the density of tracks above the subtropical high east of the California upwelling system and a spread of the density both north and south.

This weakening and poleward shift of anticyclone activity may be associated with a weakening of the Hadley circulation, which we see in our Pliocene simulations and which has been associated with poleward shifts of the storm tracks in simulations of future global warming. Another potential factor is a reduction of the meridional SST gradient, and a poleward shift of the maximum gradient. This would reduce the energy available to midlatitude anticyclones, and may explain their reduced frequency and intensity.

An important caveat is that we have focused on upwelling-favorable wind events here, yet the use of an atmosphere-only model in this study does not allow us to study the effects of a different thermocline depth. The same wind will lead to a different SST and proxy upwelling signal, and this was explored by Miller and Tziperman (2017). We emphasize that the mechanism explored here involves the basin-scale SST gradient altering synoptic-scale wind patterns. While localized changes in SST due to upwelling may modify the winds, the effect is expected to be secondary.

There is evidence that strong upwelling-favorable wind events are responsible for most of the upwelling impact on sea surface temperature and most of the effect on biological productivity which is recorded in proxy records. Our results that these wind events decrease significantly for Pliocene-like SSTs are a step toward explaining the Pliocene SST signal and toward understanding possible future changes to coastal upwelling zones.

Acknowledgments

We thank two anonymous reviewers and associate editor Chris Poulsen for most helpful comments. This work was funded by the NSF P2C2 program, grant OCE-1602864, and by the Harvard Global Institute. ET thanks the Weizmann Institute for its hospitality during parts of this work. We would like to acknowledge high-performance computing support from Cheyenne provided by NCAR's Computational and Information Systems Laboratory, sponsored by the National Science Foundation. Data availability: all GCM input files used to produce the runs analyzed in the manuscript, post processing scripts used for the analysis are available under `https://osf.io/` and under `http://www.seas.harvard.edu/climate/eli/Downloads/`.

References

Allen, J. (1980). Models of wind-driven currents on the continental shelf. *Annual Review of Fluid Mechanics*, *12*(1), 389–433.

Arnold, N., & Tziperman, E. (2015). Reductions in mid-latitude upwelling-favorable winds implied by weaker large-scale Pliocene SST gradients. *Paleoceanography*, *30*, 1-13, doi:10.1002/2015PA002806.

Bakun, A., & Nelson, C. S. (1991). The seasonal cycle of wind-stress curl in subtropical eastern boundary current regions. *Journal of Physical Oceanography*, *21*(12), 1815–1834.

Boccaletti, G., Pacanowski, R., Philander, S., & Fedorov, A. (2004). The Thermal Structure of the Upper Ocean. *J. Phys. Oceanogr.*, *34*(4), 888–902.

Botsford, L. W., Lawrence, C. A., Dever, E. P., Hastings, A., & Largier, J. (2006). Effects of variable winds on biological productivity on continental shelves in coastal upwelling systems. *Deep Sea Research Part II: Topical Studies in Oceanography*, *53*(25-26), 3116–3140.

Brierley, C. M., Fedorov, A. V., Liu, Z., Herbert, T. D., Lawrence, K. T., & LaRiviere, J. P. (2009, MAR 27). Greatly expanded tropical warm pool and weak-

ened hadley circulation in the early pliocene. *Science*, *323*(5922), 1714-1718. doi: 10.1126/science.1167625

Burls, N., & Fedorov, A. (2014). Simulating Pliocene warmth and a permanent El Niño-like state: The role of cloud albedo. *Paleoceanography*, *29*(10), 893–910.

Burls, N. J., & Fedorov, A. V. (2017). Wetter subtropics in a warmer world: Contrasting past and future hydrological cycles. *Proceedings of the National Academy of Sciences*, *114*(49), 12888–12893.

Cane, M., & Molnar, P. (2001). Closing of the indonesian seaway as a precursor to east african aridification around 3-4 million years ago. *Nature*, *411*, 157-162.

Capet, X. J., Marchesiello, P., & McWilliams, J. (2004). Upwelling response to coastal wind profiles. *Geophys. Res. Lett.*, *31*(13). doi: 10.1029/2004GL020123

Chaisson, W. P., & Ravelo, A. C. (2000, October). Pliocene development of the east-west hydrographic gradient in the equatorial Pacific. *Paleoceanography*, *15*(5), 497-505.

Chandler, M., Rind, D., & Thompson, R. (1994, DEC). Joint investigations of the middle Pliocene climate .2. GISS GCM northern-hemisphere results. *Global and Planetary Change*, *9*(3-4), 197-219. doi: 10.1016/0921-8181(94)90016-7

Dekens, P. S., Ravelo, A. C., & McCarthy, M. D. (2007, AUG 10). Warm upwelling regions in the Pliocene warm period. *Paleoceanography*, *22*(3). doi: 10.1029/2006PA001394

Dekens, P. S., Ravelo, A. C., McCarthy, M. D., & Edwards, C. A. (2008). A 5 million year comparison of mg/ca and alkenone paleothermometers. *Geochemistry, Geophysics, Geosystems*, *9*(10).

Dowsett, H., Barron, J., & Poore, R. (1996, APR). Middle pliocene sea surface temperatures: A global reconstruction. *Marine Micropaleontology*, *27*(1-4), 13-25. doi: 10.1016/0377-8398(95)00050-X

Dowsett, H., & Robinson, M. M. (2009). Mid-Pliocene equatorial sea surface temperature reconstruction: a multi-proxy perspective. *Phil. Trans. R. Soc.*, *367*(1886), 109-125, doi: 10.1098/rsta.2008.0206.

Dowsett, H. J., Foley, K. M., Stoll, D. K., Chandler, M. A., Sohl, L. E., Bentsen, M., ... Zhang, Z. (2013). Sea surface temperature of the mid-piacenzian ocean: A data-model comparison. *Scientific reports*, *3*.

Dowsett, H. J., Haywood, A. M., Valdes, P. J., Robinson, M. M., Lunt, D. J., Hill, D., ... Foley, K. M. (2011, AUG 15). Sea surface temperatures of the mid-piacenzian warm period: A comparison of prism3 and hadcm3. *Palaeogeography Palaeoclimatology Palaeoecology*, *309*(1-2, SI), 83-91. doi: 10.1016/j.palaeo.2011.03.016

Dowsett, H. J., Robinson, M. M., Haywood, A. M., Hill, D. J., Dolan, A. M., Stoll, D. K., ... Riesselman, C. R. (2012, MAY). Assessing confidence in pliocene sea surface temperatures to evaluate predictive models. *Nature Climate Change*, *2*(5), 365-371. doi: 10.1038/NCLIMATE1455

Dugdale, R., Wilkerson, F., Hogue, V., & Marchi, A. (2006). Nutrient controls on new production in the bodega bay, california, coastal upwelling plume. *Deep Sea Research Part II: Topical Studies in Oceanography*, *53*(25-26), 3049–3062.

Enriquez, A., & Friehe, C. (1995). Effects of wind stress and wind stress curl variability on coastal upwelling. *Journal of Physical Oceanography*, *25*(7), 1651–1671.

Fedorov, A., Brierley, C., Lawrence, K., Liu, Z., Dekens, P., & Ravelo, A. (2013). Patterns and mechanisms of early Pliocene warmth. *Nature*, *496*(7443), 43–49.

Fedorov, A., Dekens, P., McCarthy, M., Ravelo, A., deMenocal, P., Barreiro, M., ... Philander, S. (2006, JUN 9). The Pliocene paradox (mechanisms for a permanent El Niño). *Science*, *312*(5779), 1485-1489. doi: 10.1126/science.1122666

Fedorov, A. V., Brierley, C. M., & Emanuel, K. (2010, FEB 25). Tropical cyclones

and permanent el nino in the early pliocene epoch. *Nature*, *463*(7284), 1066-U84. doi: 10.1038/nature08831

Ford, H. L., Ravelo, A. C., Dekens, P. S., LaRiviere, J. P., & Wara, M. W. (2015). The evolution of the equatorial thermocline and the early pliocene el padre mean state. *Geophysical Research Letters*, *42*(12), 4878–4887.

Frierson, D. M., Held, I. M., & Zurita-Gotor, P. (2006). A gray-radiation aquaplanet moist gcm. part i: Static stability and eddy scale. *Journal of the Atmospheric Sciences*, *63*(10), 2548–2566.

García-Reyes, M., & Largier, J. (2010). Observations of increased wind-driven coastal upwelling off central california. *Journal of Geophysical Research: Oceans*, *115*(C4).

Haug, G. H., Sigman, D. M., Tiedemann, R., Pedersen, T. F., & Sarnthein, M. (1999). Onset of permanent stratification in the subarctic pacific ocean. *Nature*, *401*(6755), 779.

Haywood, A., Hill, D., Dolan, A., Otto-Bliesner, B., Bragg, F., Chan, W., ... Zhang, Z. (2012). Large-scale features of pliocene climate: results from the pliocene model intercomparison project. *Climate of the Past Discussions*, *8*, 2969–3013.

Haywood, A. M., Valdes, P. J., & Peck, V. L. (2007, feb 27). A permanent El Niño-like state during the Pliocene? *Paleoceanography*, *22*(1).

Herbert, T. D., & Schuffert, J. D. (1998). Alkenone unsaturation estimates of late Miocene through late Pliocene sea surface temperatures at Site 958. *Proc. Ocean Drill. Program Sci. Results*, *159T*, 17–21.

Hodges, K. (1994). A general method for tracking analysis and its application to meteorological data. *Monthly Weather Review*, *122*(11), 2573–2586.

Hodges, K. (1995). Feature tracking on the unit sphere. *Monthly Weather Review*, *123*(12), 3458–3465.

Hodges, K. (1996). Spherical nonparametric estimators applied to the ugamp model integration for amip. *Monthly Weather Review*, *124*(12), 2914–2932.

Hurlburt, H., & Thompson, J. D. (1973). Coastal upwelling on a β-plane. *J. Phys. Oceanogr.*, *3*(1), 16–32.

Koll, D. D., & Abbot, D. S. (2013). Why tropical sea surface temperature is insensitive to ocean heat transport changes. *Journal of Climate*, *26*(18), 6742–6749.

Largier, J. L., Lawrence, C., Roughan, M., Kaplan, D., Dever, E., Dorman, C., ... others (2006). West: A northern california study of the role of wind-driven transport in the productivity of coastal plankton communities. *Deep Sea Research Part II: Topical Studies in Oceanography*, *53*(25-26), 2833–2849.

LaRiviere, J. P., Ravelo, A. C., Crimmins, A., Dekens, P. S., Ford, H. L., Lyle, M., & Wara, M. W. (2012). Late Miocene decoupling of oceanic warmth and atmospheric carbon dioxide forcing. *Nature*, *486*. doi: 10.1038/nature11200

Lau, K., & Shen, S. (1988). On the dynamics of intraseasonal oscillations and enso. *Journal of the atmospheric sciences*, *45*(12), 1781–1797.

Lawrence, D. M., Oleson, K. W., Flanner, M. G., Thornton, P. E., Swenson, S. C., Lawrence, P. J., ... others (2011). Parameterization improvements and functional and structural advances in version 4 of the community land model. *Journal of Advances in Modeling Earth Systems*, *3*(1).

Lu, J., Vecchi, G. A., & Reichler, T. (2007). Expansion of the hadley cell under global warming. *Geophys. Res. Lett.*, *34*(6).

Marlow, J. R., Lange, C., Wefer, G., & Rosell-Mele, A. (2000). Upwelling intensification as part of the Pliocene-Pleistocence climate transition. *Science*, *290*, 2288-2291.

Marshall, J., & Plumb, R. A. (2016). *Atmosphere, ocean and climate dynamics: an introductory text* (Vol. 21). Academic Press.

Miller, M. D., & Tziperman, E. (2017). The effect of changes in surface winds and ocean stratification on coastal upwelling and sea surface temperatures in the

Pliocene. *Paleoceanography*, *32*(doi:10.1002/2016PA002996), 371-383.

Mitas, C. M., & Clement, A. (2006). Recent behavior of the hadley cell and tropical thermodynamics in climate models and reanalyses. *Geophysical Research Letters*, *33*(1).

Neale, R. B., Chen, C.-C., Gettelman, A., Lauritzen, P. H., Park, S., Williamson, D. L., ... others (2010). Description of the ncar community atmosphere model (cam 5.0). *NCAR Tech. Note NCAR/TN-486+ STR*, *1*(1), 1–12.

Neale, R. B., Chen, C.-C., Gettelman, A., Lauritzen, P. H., Park, S., Williamson, D. L., ... Taylor, M. A. (2012, November). *Description of the ncar community atmosphere model (cam 5.0)* (Tech. Rep. Nos. technical note NCAR/TN-486+STR). Boulder, Colorado, USA: National Center for Atmospheric Research.

O'Brien, C. L., Foster, G. L., Martínez-Botí, M. A., Abell, R., Rae, J. W., & Pancost, R. D. (2014). High sea surface temperatures in tropical warm pools during the pliocene. *Nature Geoscience*, *7*(8), 606–611.

Oleson, K., Lawrence, D., Bonan, G., Flanner, M., Kluzek, E., Lawrence, P., ... others (2010). Technical description of version 4.0 of the community land model (clm), ncar tech. *Notes (NCAR/TN-478+ STR)*.

Pauly, D., & Christensen, V. (1995). Primary production required to sustain global fisheries. *Nature*, *374*(March), 255–257.

Philander, S., & Fedorov, A. (2003, JUN 5). Role of tropics in changing the response to milankovich forcing some three million years ago. *Paleoceanography*, *18*(2). doi: 10.1029/2002PA000837

Ravelo, A. C., Dekens, P. S., & McCarthy, M. (2006). Evidence for el niño-like conditions during the pliocene. *Gsa Today*, *16*(3), 4.

Rayner, N., Parker, D. E., Horton, E., Folland, C., Alexander, L., Rowell, D., ... Kaplan, A. (2003). Global analyses of sea surface temperature, sea ice, and night marine air temperature since the late nineteenth century. *Journal of Geophysical Research: Atmospheres*, *108*(D14).

Renault, L., Dewitte, B., Marchesiello, P., Illig, S., Echevin, V., Cambon, G., ... Ayers, J. K. (2012). Upwelling response to atmospheric coastal jets off central chile: A modeling study of the october 2000 event. *Journal of Geophysical Research: Oceans*, *117*(C2).

Schneider, E. K. (1977). Axially symmetric steady-state models of the basic state for instability and climate studies. Part II: non-linear calculations. *J. Atmos. Sci.*, *34*, 280-296.

Seager, R., Murtugudde, R., Naik, N., Clement, A., Gordon, N., & Miller, J. (2003). Air–sea interaction and the seasonal cycle of the subtropical anticyclones. *Journal of climate*, *16*(12), 1948–1966.

Small, R. J., Curchitser, E., Hedstrom, K., Kauffman, B., & Large, W. G. (2015). The benguela upwelling system: Quantifying the sensitivity to resolution and coastal wind representation in a global climate model. *Journal of Climate*, *28*(23), 9409–9432.

Spall, M. A., & Schneider, N. (2016). Coupled ocean/atmosphere offshore decay scale of cold SST signals along upwelling eastern boundaries. *Journal of Climate*, *in press*. doi: 10.1175/JCLI-D-16-0109.1

Steph, S., Tiedemann, R., Prange, M., Groeneveld, J., Schulz, M., Timmermann, A., ... Haug, G. H. (2010). Early pliocene increase in thermohaline overturning: A precondition for the development of the modern equatorial pacific cold tongue. *Paleoceanography*, *25*(2). doi: 10.1029/2008PA001645

Tierney, J. E., Haywood, A. M., Feng, R., Bhattacharya, T., & Otto-Bliesner, B. L. (2019). Pliocene warmth consistent with greenhouse gas forcing. *Geophysical Research Letters*, *46*(15), 9136–9144.

Tziperman, E., & Farrell, B. F. (2009). The Pliocene equatorial temperature — lessons from atmospheric superrotation. *Paleoceanography*, *24*, PA1101,

doi:10.1029/2008PA001652.

Walker, C. C., & Schneider, T. (2006). Eddy influences on hadley circulations: Simulations with an idealized gcm. *Journal of the atmospheric sciences*, *63*(12), 3333–3350.

Wara, M., Ravelo, A., & Delaney, M. (2005, JUL 29). Permanent El Niño-like conditions during the Pliocene warm period. *Science*, *309*(5735), 758-761. doi: 10 .1126/science.1112596

Wilkerson, F. P., Lassiter, A. M., Dugdale, R. C., Marchi, A., & Hogue, V. E. (2006). The phytoplankton bloom response to wind events and upwelled nutrients during the coop west study. *Deep Sea Research Part II: Topical Studies in Oceanography*, *53*(25-26), 3023–3048.

Winant, C. D., & Dorman, C. E. (1997). Seasonal patterns of surface wind stress and heat flux over the southern california bight. *Journal of Geophysical Research: Oceans*, *102*(C3), 5641–5653.

Zhang, Y. G., Pagani, M., & Liu, Z. (2014). A 12-million-year temperature history of the tropical pacific ocean. *science*, *344*(6179), 84–87.

Table 1. Annual Mean Intensity upwelling intensity and reductions for Pliocene SST scenarios, see text for details.

Resolution	Case	Coastal Upwelling Index ($\mathrm{ton\,m^{-1}\,s^{-1}}$)	Offshore Upwelling Index ($g\,m^{-2}\,s^{-1}$)	Reduction of Coastal Upwelling	Reduction of Offshore Upwelling
1 degree	Modern	1.061	2.875		
	PRISM4	0.939	2.665	11.5%	7.3%
	Idealized	0.654	1.635	38.4%	43.1%
0.5 degree	Modern	1.251	2.895		
	PRISM4	1.163	2.813	7.0%	2.8%
	Idealized	0.784	1.522	37.3%	47.4%
0.25 degree	Modern	1.423	3.323		
	PRISM4	1.260	2.958	11.5%	11.0%
	Idealized	0.804	1.791	43.5%	46.1%

Table 2. Duration and intensity of strong upwelling events and total reduction in annual upwelling flux in strong events for Pliocene SST scenarios, see text for details.

Resolution	Case	Events per year	Total event duration per year (days)	Average duration (days)	Average flux ($\mathrm{ton\,m^{-1}s^{-1}}$)	Annual flux reduction (%)
1 degree	Modern	22.2	231.7	10.5	1.438	
	PRISM4	26.3	227.2	8.7	1.273	13.2%
	Idealized	21.8	157.9	7.3	1.119	47.0%
0.5 degree	Modern	25.1	243.0	9.7	1.629	
	PRISM4	25.2	247.6	9.8	1.481	7.4%
	Idealized	24.3	171.3	7.1	1.231	46.7%
0.25 degree	Modern	28.5	248.5	8.7	1.811	
	PRISM4	28.5	238.5	8.4	1.688	10.5%
	Idealized	29.0	168.0	5.8	1.330	50.3%

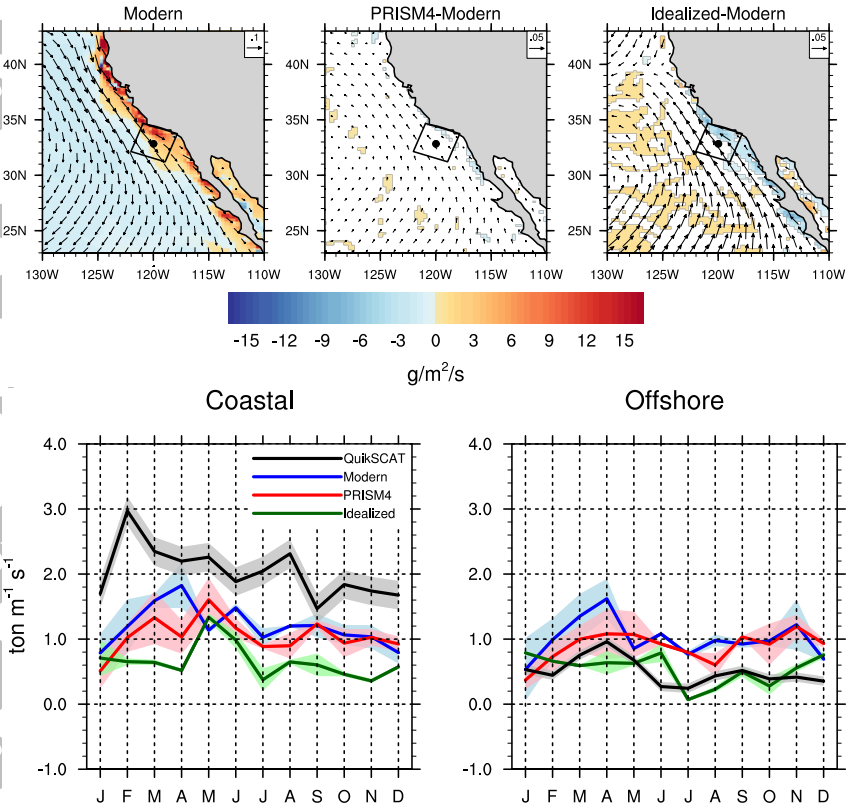

Figure 1. Annual mean and seasonal response to SST scenarios. (Upper panels) Annual mean surface wind stress (vectors) and upwelling estimated via wind stress curl (shadings), for all three SST configurations, using the 0.25° resolution atmospheric model. Shown are the CAM5 simulation with modern SST (left), the difference between PRISM4 and modern SST (middle), and the difference between idealized and modern SST (right). Upwelling units are $g\,m^{-2}\,s^{-1}$ with a shared color scale. Statistically insignificant (95%) differences appear white, based on the Student's t test. A 0.1 $\mathrm{N\,m^{-2}}$ (modern) and 0.05 $\mathrm{N\,m^{-2}}$ (differences) reference vector is shown in the up right of each panel. (Lower panels) Monthly indices for coastal and curl-driven upwelling around the California sediment core Site 1014, for the modern (blue), PRISM4 (red) and idealized (green) cases, with QuikSCAT wind results shown by the black curves. Indices are based on average alongshore wind stress (coastal), or the average of the wind stress curl (offshore) within a 300 km square box around the sediment core site multiplied by 300 km to bring it to the same units as the coastal index. Shading indicates ±1 standard error.

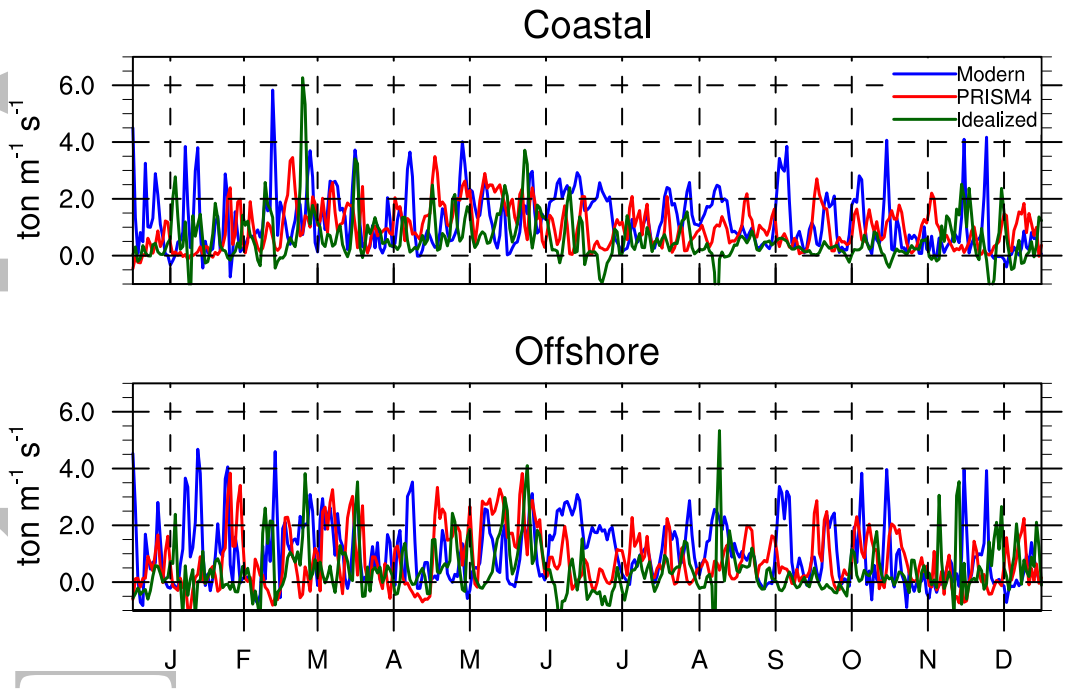

Figure 2. Daily indices for coastal and offshore upwelling around California site, for the modern (blue), PRISM4 (red) and idealized (green) cases. Both indices are calculated by daily wind stress data from the last year of the 1° simulations.

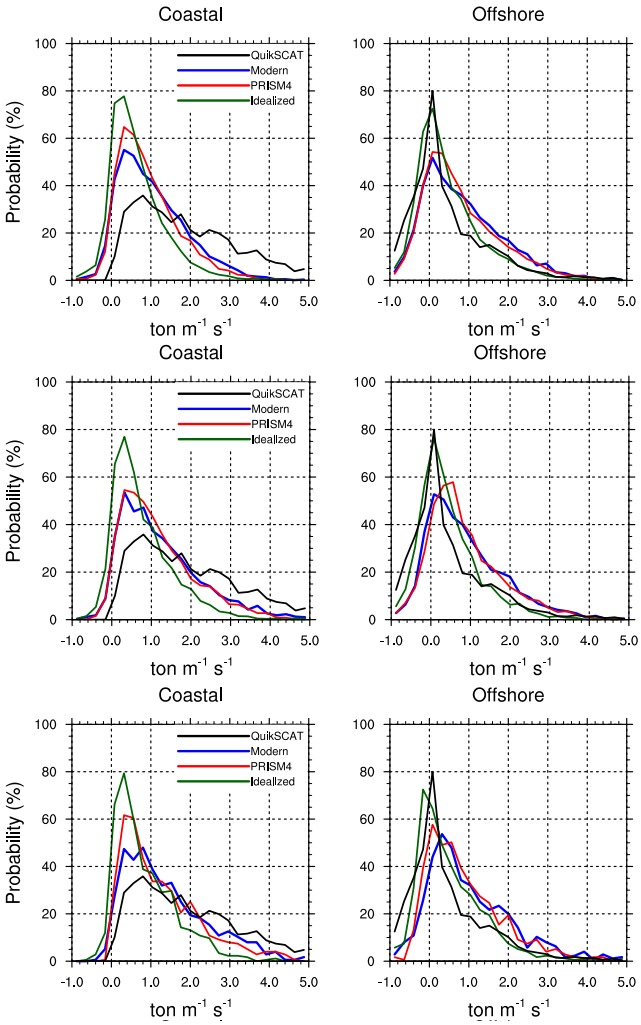

Figure 3. Probability distribution function for daily coastal and offshore upwelling indices, for the modern (blue), PRISM4 (red) and idealized (green) cases, derived from the final 10 years of the 1° and 0.5° simulations, and the final year of the 0.25° simulation.

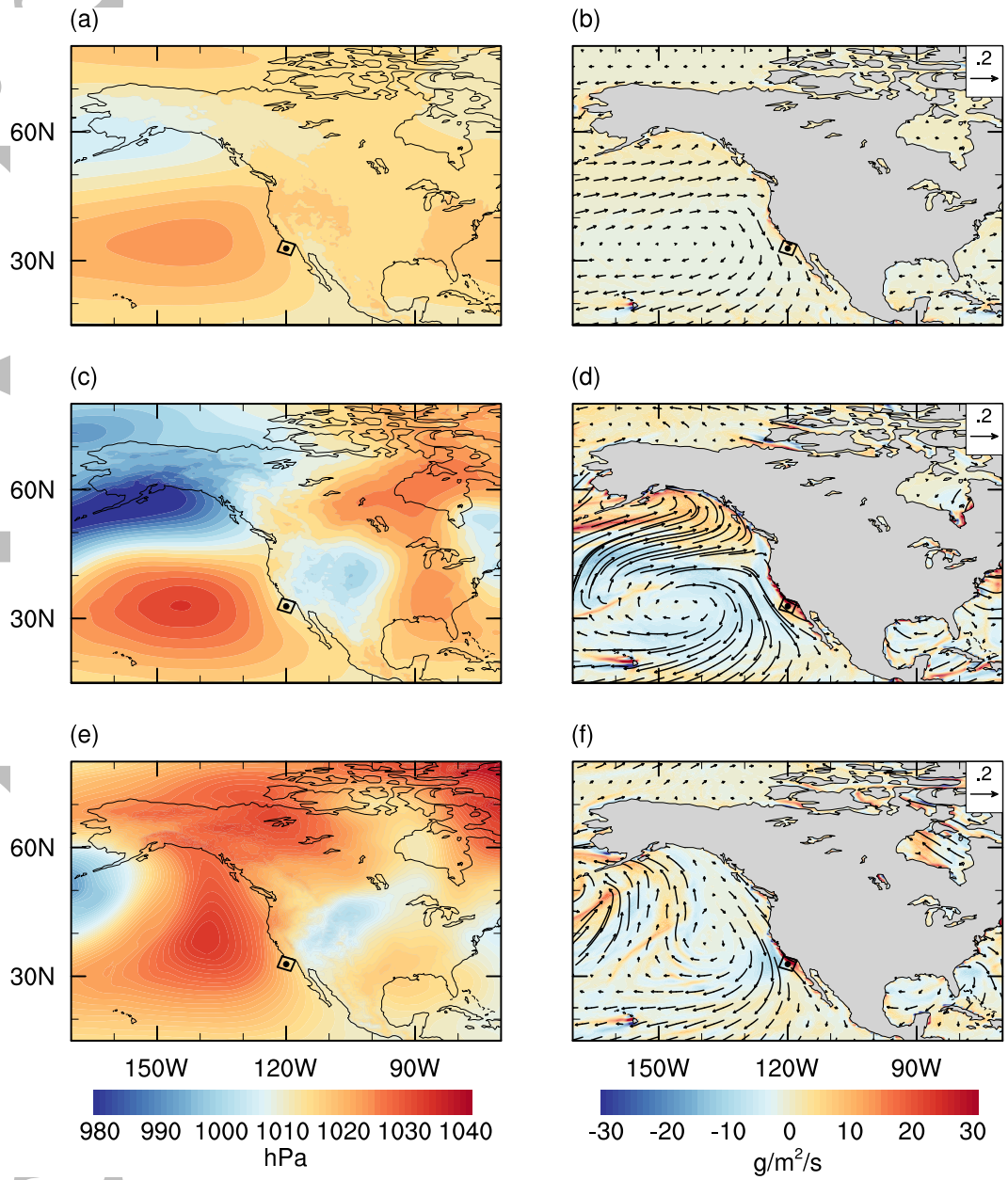

Figure 4. Sea level pressure (left column) and surface wind stress and offshore upwelling due to wind stress curl (right column). (Upper row) climatology. (Middle row) same, during the event corresponding to largest coastal upwelling index value. (Bottom row) same, for the second largest event.

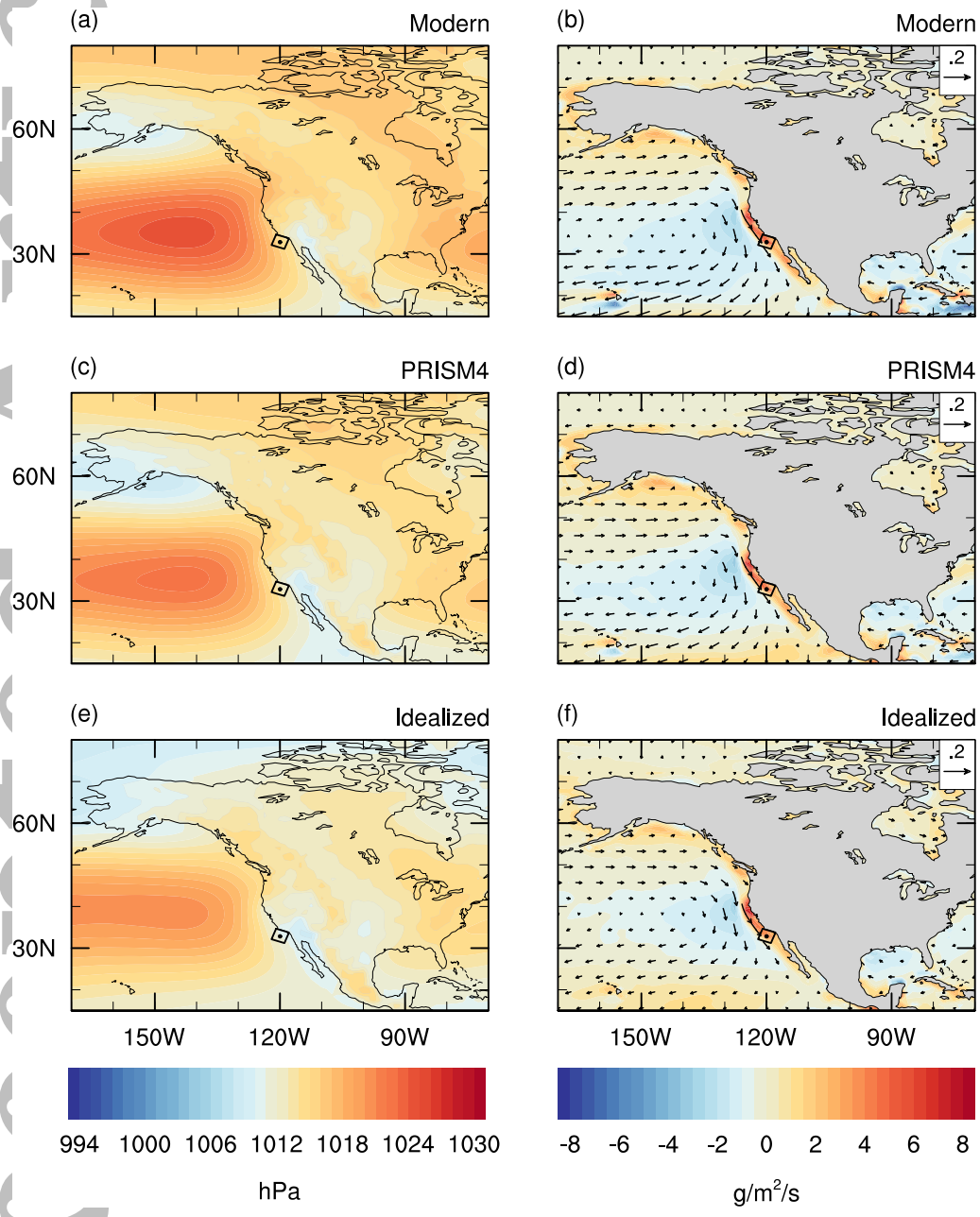

Figure 5. Composite for strong upwelling events of sea level pressure (left column) and surface wind stress and curl-driven upwelling mass flux (right column), for modern (top row), PRISM4 (middle row) and idealized (bottom row) cases. Strong events are defined to be those with a duration over 3 days whose alongshore wind velocity exceeds 5 m s^{-1}.

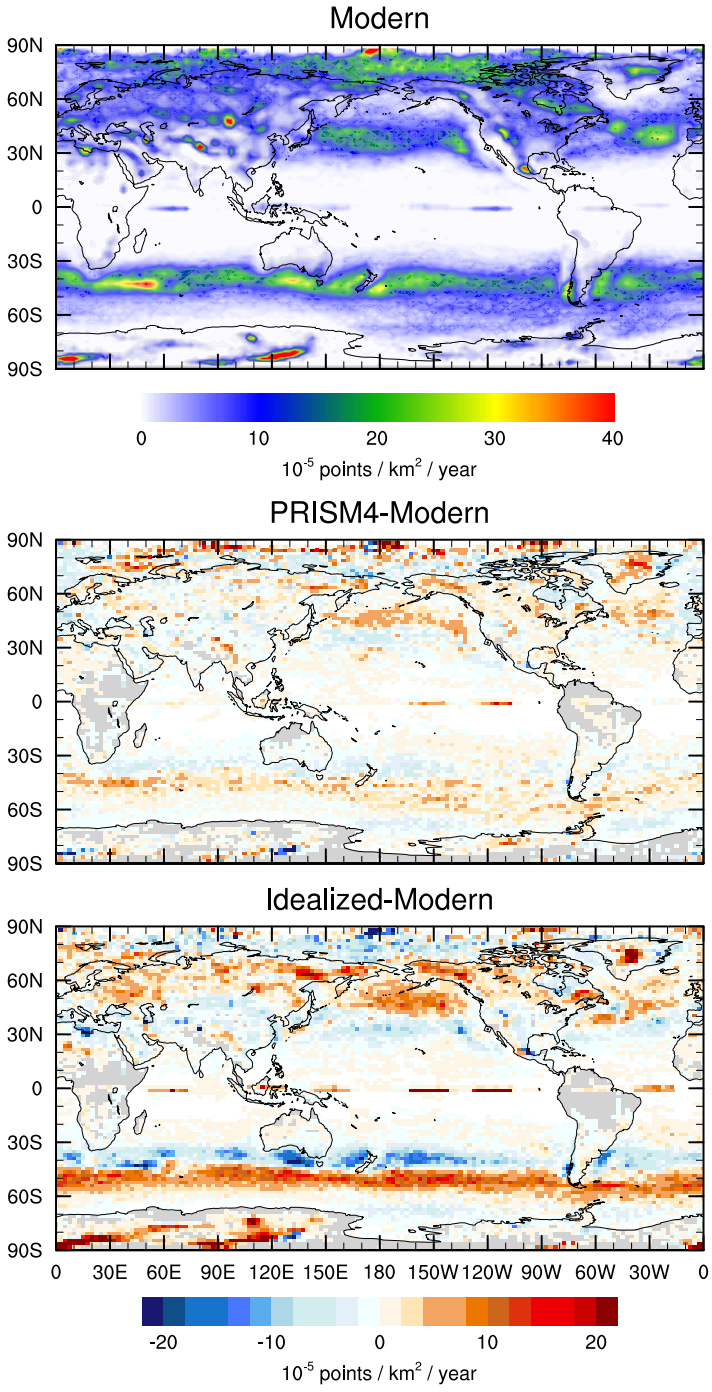

Figure 6. Anticyclone tracks and track density in the three SST scenarios using the 1° resolution model based on a 20 year run. Track point density for the modern SST (top). The difference between the track density for PRISM4 and modern SST (middle). The difference between idealized and modern SST (bottom). Grid points with no anticyclone track points appear white.

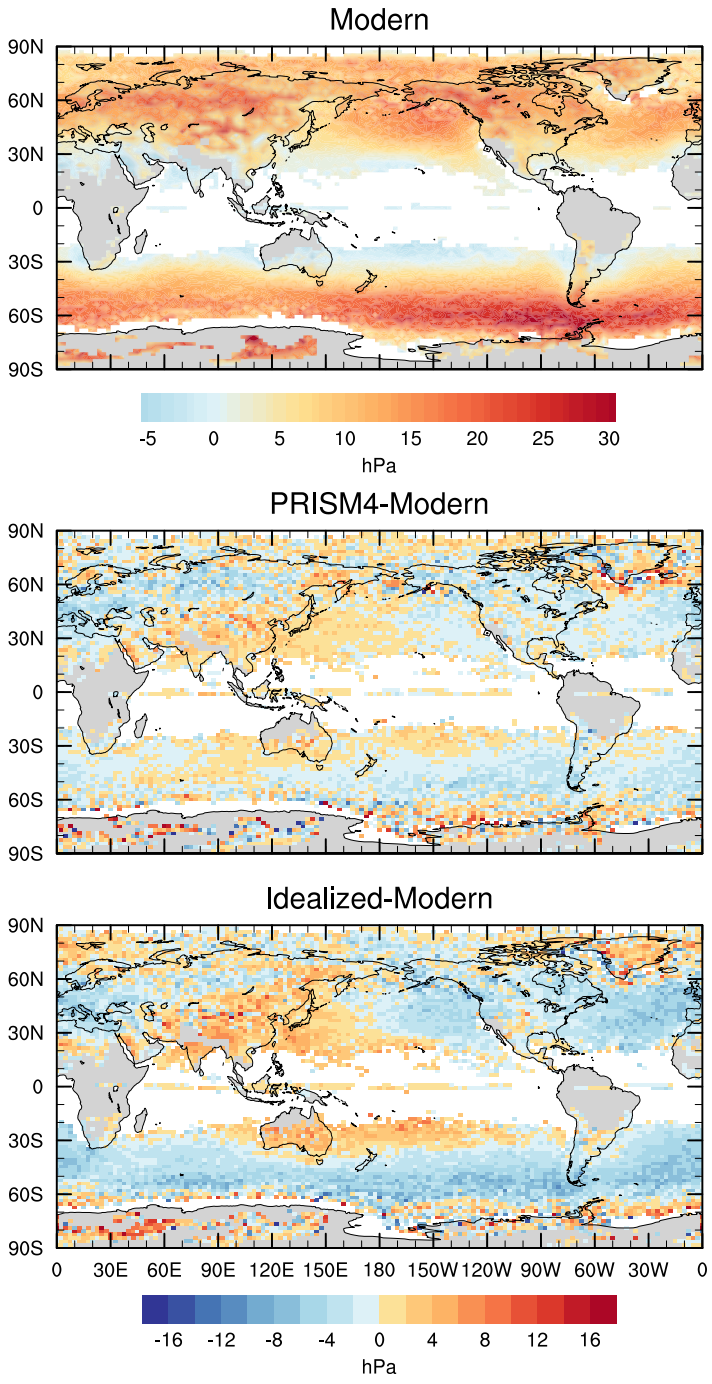

Figure 7. The intensity of anticyclones whose tracks are shown in Fig. 6. (a) The intensity of anticyclones for the modern SST (top). The difference between the intensity of anticyclone for PRISM4 and modern SST (middle). The difference between idealized and modern SST (bottom). Grid points with no anticyclone track points appear white.